DEUTSCHES ELEKTRONEN-SYNCHROTRON **DESY**

DESY 86-078
July 1986

INCLUSIVE π^0 PRODUCTION BY e^+e^- ANNIHILATION AT 34.6 GeV CENTER OF MASS ENERGY

by

TASSO Collaboration

ISSN 0418-9833

NOTKESTRASSE 85 · 2 HAMBURG 52

To be sure that your preprints are promptly included in the
HIGH ENERGY PHYSICS INDEX ,
send them to the following address (if possible by air mail) :

DESY
Bibliothek
Notkestrasse 85
2 Hamburg 52
Germany

DESY 86-078
July 1986

ISSN 0418-9833

Inclusive π^0 Production by e^+e^- Annihilation at 34.6 GeV Center of Mass Energy

TASSO Collaboration

W. Braunschweig, R. Gerhards, F.J. Kirschfink, H.-U. Martyn, P. Rosskamp, E. Vogel, W. Wallraff
I. Physikalisches Institut der RWTH Aachen, Germany[15]

B. Bock, J. Eisenmann, H.M. Fischer, H. Hartmann, E. Hilger, A. Jocksch, H. Kolanoski, H. Kück[1], V. Mertens, R. Wedemeyer
Physikalisches Institut der Universität Bonn, Germany[15]

B. Foster, A.J. Martin
H.H. Wills Physics Laboratory, University of Bristol, Bristol, UK[16]

E. Bernardi, Y. Eisenberg[2], A. Eskreys[3], K. Gather, H. Hultschig, P. Joos, B. Klima, H. Kowalski, A. Ladage, B. Löhr, D. Lüke, P. Mättig[4], A. Montag, D. Notz, A. Shapira[2], D. Trines, T. Tymieniecka[5], G. Tysarczyk, R. Walczak[6], G. Wolf, G. Yekutieli[2], W. Zeuner
Deutsches Elektronen-Synchrotron DESY, Hamburg, Germany

T. Kracht, H.L. Krasemann[7], J. Krueger, E. Lohrmann, G. Poelz, K.-U. Poesnecker
II. Institut für Experimentalphysik der Universität Hamburg, Germany[15]

D.M. Binnie, P.J. Dornan, D.A. Garbutt, C. Jenkins[8], W.G. Jones, J.K. Sedgbeer, J. Shulman, D. Su, A.P. Watson
Department of Physics, Imperial College London, UK[16]

F. Barreiro, E. Ros
Universidad Autonoma de Madrid, Madrid, Spain[19]

C. Balkwill, M.G. Bowler, P.N. Burrows, R.J. Cashmore, P. Dauncey, R. Devenish, G. Heath, D.J. Mellor, P. Ratoff, I. Tomalin, J.M. Yelton
Department of Nuclear Physics, Oxford University, Oxford, UK[16]

S.L. Lloyd
Department of Physics, Queen Mary College, London, UK[16]

G.E. Forden, J.C. Hart, D.K. Hasell[9], D.H. Saxon
Rutherford Appleton Laboratory, Chilton, Didcot, UK[16]

S. Brandt, M. Holder, L. Labarga[10], B. Neumann
Fachbereich Physik der Universität-Gesamthochschule Siegen, Germany[15]

U. Karshon, G. Mikenberg, R. Mir, D. Revel, E. Ronat, N. Wainer
Weizmann Institute, Rehovot, Israel[17]

G. Baranko[11], A. Caldwell, M. Cherney[12], J.M. Izen[13], S. Ritz, D. Strom, M. Takashima, E. Wicklund[14], Sau Lan Wu, G. Zobernig
Department of Physics, University of Wisconsin, Madison, Wisconsin, USA[18]

1) Now at Fraunhofer Institut, Duisburg, Germany
2) On leave from Weizmann Institute, Rehovot, Israel
3) On leave from Institute of Nuclear Physics, Cracow, Poland
4) Now at IPP Canada, Carleton University, Ottawa, Canada
5) Now at Warsaw University, Poland
6) On leave from Warsaw University, Poland
7) Now at GKSS, Geesthacht, Germany
8) Now at Logica Ltd.
9) Now at IPP Canada, York University, Toronto, Canada
10) On leave from Universidad Autonómia de Madrid, Madrid, Spain
11) Now at University of Colorado, Boulder, CO, USA
12) Now at Lawrence Berkeley Laboratory, Berkeley, CA, USA
13) Now at University of Illinois at Urbana-Champaign, Urbana, IL, USA
14) Now at California Institute of Technology, Pasadena, CA, USA
15) Supported by the Bundesministerium für Forschung und Technologie
16) Supported by the UK Science and Engineering Research Council
17) Supported by the Minerva Gesellschaft für Forschung GmbH.
18) Supported by the US Department of Energy, contract DE-AC02-76ER000881 and the U.S. National Science Foundation Grant Number INT-8313994 for travel
19) Supported by CAICYT

Abstract

The cross section for the process $e^+e^- \to \pi^0 +$ anything has been measured at a Center of mass energy of 34.6 GeV for π^0 energies between 0.7 and 17 GeV. The angular distribution for π^0 energies > 2 Gev is of the form $d\sigma/d\Omega \sim 1 + A \cos^2\theta$, with $A = 1.2 \pm 0.5$
The ratio of π^0 to $\pi^\pm$ production in the measured energy range is $2\,\sigma(\pi^0)/(\sigma(\pi^+) + \sigma(\pi^-)) = 1.13 \pm 0.18$
The form of the differential cross sections agrees within the errors.
The mean π^0 multiplicity is 5.8 ± 0.9.

1. Introduction

The study of hadron production in e^+e^- -annihilations at high energies gives important insight in the mechanism of the hadronisation of quarks. The TASSO collaboration has followed a program to measure rather completely the inclusive cross sections of the most frequent hadrons, such as pions, kaons, protons and Λ hyperons 1,2,3). The aim is to provide a general overview of hadron production and to determine the relative contributions of the various hadron species to the overall energy balance in e^+e^- -annihilations.

In this paper we present data on inclusive π^c cross sections which are an update of previously published results 4) employing six times higher statistics and extending the π^o momentum range. The fine granularity of the TASSO liquid argon shower counters allows an identification of π^o's up to the highest momenta at PETRA energies.

2. Experimental Procedure

2.1 Description of Detector

The experiment has been performed with the TASSO detector at the e^+e^- storage ring PETRA. An integrated luminosity of 66.8 pb^{-1} at an average center of mass energy of 34.6 GeV has been used. For the investigation reported in this paper multihadron events from e^+e^- annihilation have been selected as described in previous publications (5,6) using the charged particle information provided by the central detector. Approximately 18500 events have been used for the analysis, satisfying the selection criteria and having calorimeter information. The detector components used for charged (7) and neutral (4,8,9,10) particle detection have been described previously. This analysis is based on photons from π^o decay detected in lead-liquid argon barrel and endcap calorimeters. We briefly review the main features of the calorimeters below.

The barrel calorimeters are located above and below the magnet coil. They cover 40 % of solid angle extending from $42° \lesssim \theta \lesssim 138°$ in polar angle in two sections of azimuthal angle, namely $30° \lesssim \phi \lesssim 150°$ and $210° < \phi < 330°$. They consist of a system of towers and strips. The towers are composed of 2 mm thick lead plates of area $\cong$ 7 x 7 cm^2 (front towers) and $\cong$ 14 x 14 cm^2 (back towers) stacked so as to point at the interaction region. Four front towers are followed by one back tower. The strips are $\cong$ 2 cm wide and etched on copper clad epoxy circuit board. They run orthogonal to the beam axis (z = constant) and parallel to it (ϕ = constant). The first active layer of the calorimeter is at a radial distance of 178 cm from the interaction point. The front towers contain 6.1 radiation lengths of material, the back towers 7.6 radiation lengths. There are 1.3 radiation lengths of material before the first active layer of the calorimeter. The towers provide a measurement of the total energy of electromagnetic showers with a resolution determined from electrons (8) with energy 1 < E < 5 GeV of $\sigma_E/E = \frac{0.136}{\sqrt{E}} + 0.03$, (E in GeV). The electronic threshold of the towers corresponds to a shower energy of 18 MeV. The strips provide a position resolution determined from electrons (8) with energy 1 < E < 5 GeV of σ = (0.77/E + 0.53) cm, (E in GeV). The energy calibration has been carried out with electrons of energy 17.3 GeV from Bhabha scattering ($e^+e^- \to e^+e^-$) events. The detection efficiency for isolated photons has been determined from EGS Monte Carlo studies (11) to be 50 % at 0.055 GeV rising to > 90 % above 0.160 GeV.

The endcap calorimeters cover polar angles of $12° \lesssim \theta \lesssim 29°$ and $151° \lesssim \theta < 168°$ over the full azimuth. They consist of front towers (5.9 radiation lengths),

back towers (7.6 radiation lengths) and strips. The towers and strips are shaped as circular segments. The front towers have a constant azimuthal size of $\Delta\phi = 5°$ and a radial size chosen so that the solid angle subtended is $\cong$ 0.7 mster. Four front towers are followed by one back tower. The radial strips have half the front tower width ($\cong$ 2.5 cm) and the azimuthal strips have half the front tower azimuthal angle (2.5°). The first active layer of the endcap calorimeters is located at a distance of 191 cm from the interaction point in the beam direction. There is 1.0 radiation length of material in front of the calorimeters at normal incidence. The energy calibration, energy resolution and angular resolution have been measured with electrons of energy $7 \lesssim E \lesssim 18$ GeV from Bhabha scattering events. Since these measurements are well reproduced by EGS Monte Carlo simulations, we used the simulations to determine the energy and angular resolutions below 7 GeV. The energy resolution can be parameterized as $\sigma_{E/E} = 0.18/\sqrt{E} + 0.03$, for E < 5 GeV, E in GeV. The azimuthal (polar) angular resolution for photons is σ_ϕ = 15 mrad (σ_θ = 7 mrad) at E = 0.2 GeV, and improves to a constant value of σ_ϕ = 11 mrad (σ_θ = 4 mrad) for E > 1 GeV. The reconstruction efficiency for isolated photons is 25 % at photon energies of 0.2 GeV and greater than 90 % at photon energies above 0.4 GeV. As the two calorimeter systems have different systematic errors, and are separated by a gap of 13° in polar angle we have not attempted to combine photons from the barrel and endcap calorimeters to form π^o mesons.

2.2 Detection of π^o Mesons

2.2.1 Barrel Calorimeter ($E_{\pi^o} < 6$ GeV)

We first describe the analysis procedure for the barrel calorimeters. As in the previous analysis 4,12), photons are recognized in the calorimeters as clusters of deposited energy. The cluster search starts from a local energy maximum in the front towers. A connected region is constructed by successively combining all front towers, above the hardware energy threshold, which share a common side. Towers which only abut diagonally are not included. Back towers which lie behind the front tower of the cluster are associated with the front tower cluster and their energy is added to that of the front towers to give the total energy. Clusters which fall within 50 mrad of a charged track are removed from the photon sample. The measured energy is corrected for energy loss through absorption and leakage with correction functions determined by EGS. To ensure a good energy resolution the center of the cluster is required to be at least 37 mrad from the edge of the calorimeter. A good position accuracy is ensured by requiring information from the z and ϕ strips.

At high energies, the clusters from the two photons from π^o decay are in close proximity in the calorimeters. In order to increase the efficiency for detecting π^o mesons for energies > 2.0 GeV and as check upon the systematic errors of the measurement, an alternative cluster definition has been used in the analysis of data from the barrel calorimeters (12). This definition proceeds as the cluster finding described above, but requires a cluster to be split into two or more clusters when it is recognized that the pattern of energies deposited in the front towers is inconsistent with the pattern expected from a single photon. The results from the two definitions have been found to agree well in the energy range from 1.0 to 4.0 GeV where they overlap. The first cluster definition has been used in the range from 0.5 to 2.0 GeV and the second cluster definition for energies > 2 GeV.

For each event all possible pairs of photons have been formed and their invariant mass $m_{\gamma\gamma}$ and total energy $E_{\gamma\gamma}$ have been calculated. Each photon has been

required to have an energy of at least 0.150 GeV. For very low π^0 energies ($0.5 \leq E_{\pi^0} \leq 1.0$ GeV) the additional requirement that $E_1/(E_1+E_2) > 0.3$, where $E_1 \leq E_2$ are the photon energies, has been imposed. Figures 1a and 1b show the $m_{\gamma\gamma}$ distributions obtained at W = 34.6 GeV for $0.5 \leq E_{\gamma\gamma} \leq 4.0$ GeV from the first cluster definition and for $2.0 \leq E_{\gamma\gamma} \leq 6.0$ GeV from the second definition. Clear π^0 signals are observed. The π^0 signals are observed at $m_{\gamma\gamma} = 0.126 \pm 0.002$ GeV, which is below the o.135 GeV expected; this shift will be discussed later.

2.2.2 Barrel Calorimeter ($E_{\pi^0} > 6$ GeV)

Above 6 GeV it is not possible to reconstruct the π^0 mass from two photon clusters, because the clusters get too close. We have therefore used the lateral energy distribution of the clusters, as measured by the strips, for π^0 identification. We define the width of the lateral energy distribution along lines z = const. and Φ = const. respectively by

$$D_{\phi,z} = \left(\sum E_i (x_i - \bar{x})^2 / \sum E_i \right)^{1/2}$$

where E_i is the energy in strip i , and x_i is its position. In the case of two photons merging into one cluster a relatively large width (high dispersion D) is expected. However D should be small for clusters originating from just one photon. Fig. 2 showsthat this indeed the case. In Fig. 2a the D_ϕ and D_z distribution is plotted for single photons. Here we used our data for the reaction $e^+e^- \to \gamma\gamma$,which assures that all detector effects are taken into account. The distribution is very well reproduced by the EGS Monte Carlo simulation 13). In Fig. 2b we plot the EGS simulation for clusters to which both photons from a π^0 decay contribute. Whereas the sample from single γ's is restricted e.g. to $D_\phi < 2$cm the distribution from π^0's is broad extenting to high D_ϕ and D_z values. The difference is the basis to separate single γ's from π^0's in the data. The distribution of high energetic neutral clusters in hadronic events is displayed in Fig. 2c.Together with a clustering around small D_ϕ, D_z values the data extend to high D_ϕ and D_z values.

We have used a number of different methods to estimate the number of clusters due to two photons in the data. In a first method the number of clusters due to $\pi^0 \to \gamma\gamma$ in the experimental sample was determined by fitting it to a sum of the single-photon cluster distribution Fig. 2a and the two-photon cluster distribution Fig. 2b. We find that above 6 GeV 56 % of the clusters are two-photon clusters and the rest are due to a single photon(wide opening angle π^0decays and incorrect charged track associations).Instead of the two dimensionaldistribution D_ϕ vs. D_z we have also used the effective lateral width given by

$$R = \left[\left(D_z / \bar{D}_z \right)^2 + \left(D_\phi / \bar{D}_\phi \right)^2 \right]^{1/2}$$

The distribution of R^2 is shown in Figs. 3a-c for single photon clusters, two-photon clusters and data, respectively. Again a fit of the data to a sum of the distributions from Figs. 3a and 3b was made to determine the number of two-photon clusters in the data.

To estimate the systematic errors we have also determined this number by applying various cuts in the $D_\phi$vs. D_z distributions and comparing with the corresponding procedures in the Monte Carlo simulation. Above an energy of 4.6 GeV all methods gave consistent results (see Table 1).

2.2.3 Endcap Calorimeter

We now turn to the analysis of the data from the endcap calorimeters (14). A cluster algorithm similar to the second one described in sect. 2.2.1 for the barrel calorimeterhas been used.

. As there is no track information available in the endcap region, the discrimination between electromagnetic showering particles and hadrons has been based solely on the longitudinal shower information. A cluster is defined as a photon if a) the energy deposit in the front towers is at least 1.9 times greater than the energy deposit in the back towers, or b) if the number of associated back towers is greater than the number of front towers or c) if the reconstructed energy exceeds 0.7 GeV and at least one back tower has more than the hardware threshold energy. These criteria have been checked with data and complete Monte Carlo simulations using EGS to simulate electromagnetic showering particles and using GHEISHA (15) to simulate hadrons. The contamination of this sample by electrons is negligible. The probability of misidentifying a hadron as a photon is a smooth function with probability 0 at E = 0.3 GeV, 0.10 at E = 0.5 GeV, and 0.25 at E = 1.5 GeV. The clusters have been required to lie inside a fiducial region of $13.2^\circ \leq \theta < 27.5^\circ$ or $152.5^\circ < \theta \leq 166.8^\circ$. The reconstructed energy of each photon has been corrected for losses in front of the calorimeter using a parametrization obtained from EGS. The minimum photon energy is 0.150 GeV. Invariant masses $m_{\gamma\gamma}$ have been formed for all pairs of clusters in the same endcap. The energy of the pair has been required to be $1.5 < E_{\gamma\gamma} < 5$ GeV. A clear π^0 signal is observed as shown in Figure 1c.

2.3 Background and Efficiency

The π^0 detection efficiency as well as the shape of the background distribution in the π^0 mass region have been determined with a Monte Carlo program which simulates the response of the detector in great detail. Events have been generated for the processes

$$e^+e^- \to \text{quarks + antiquark and } e^+e^- \to \text{quark + antiquark + gluon}$$

according to first order QCD (16) using Field-Feynman fragmentation functions (17) and including radiative effects (18). For photons and electrons the shower development in the liquid argon calorimeters have been followed with the help of EGS; the shower development of hadrons in the calorimeters has also been simulated (19)(15). These simulations have produced strip and tower energies as in the experiment.

The background in the π^0 mass region has been estimated by passing the simulated events through the same analysis chain used for the real data. With these events, the loss of photons in the barrel calorimeter due to overlap with charged tracks or with other photons has been studied . The fraction of photons from π^0 decay with energy above 0.150 GeV which overlap with charged tracks or other photons is typically 23 %.

The π^0 yield has been determined between 0.7 and 17 GeV for various energy intervals. The background in the π^0 mass region has been estimated in the following way. For the barrel calorimeter the accepted photons of the Monte Carlo events were used to compute the $m_{\gamma\gamma}$ spectrum below 6 GeV excluding those pairs of photons where both γ's come from the same π^0 . The Monte Carlo spectrum has been normalized such that the number of $\gamma\gamma$- combinations with $0.250 \leq m_{\gamma\gamma} \leq 0.450$ GeV is the same as in the data. The mass resolution ensures that the contribution from π^0 decay to this mass interval is negligible. This has been done separately for each $E_{\gamma\gamma}$ interval. The dashed curves in Figures 1a and 1b show the prediction for the background obtained in this way. In Figures 4a, 4b and 4c the background-subtracted spectra are shown. A fit of a gaussian distribution to the background-subtracted spectra has been made, with the mass,

resolution and amplitude as free parameters. As stated previously, the energy calibration of the calorimeters has been determined using Bhabha scattering events. In the barrel calorimeter there is a small systematic shift in applying this calibration obtained from electrons at 17.3 GeV energy to low energy photons as the π^0 signals in the data are observed at $\gamma\gamma$ masses of about 0.126 Gev , below the 0.135 GeV expected. The π^0 signals in the Monte Carlo are observed at the expected mass. We have used two methods to account for this effect in performing the background subtraction. In the first one we have scaled then energy of the Monte Carlo photons to match the observed π^0 mass. In the second we have scaled the observed photon energies to match the known π^0 mass. Both methods agree within the errors, the differences being included in the systematic error. We have chosen the first method for the final result.

For the endcap calorimeter a fit of a gaussian distribution plus a smoothed background has been made. A π^0 r.m.s. mass resolution of $\sigma(m_{\pi^0}) = 0.026$ GeV for the barrel and $\sigma(m_{\pi^0}) = 0.023$ GeV for the endcap calorimeters are obtained. This is in good agreement with the mass resolution seen in the Monte Carlo events.

To arrive at the π^0 detection efficiency let N_1 be the number of Monte Carlo events generated at the nominal c.m. energy (i.e. without initial state radiation) and $n_1(E_{\pi^0})dE_{\pi^0}$ be the number of π^0 mesons in the Monte Carlo events in the energy range E_{π^0} to $E_{\pi^0} + dE_{\pi^0}$. Let N_2 be number of Monte Carlo events generated with radiative effects and accepted by the selection criteria for hadron events, and $n_2(E_{\pi^0})dE_{\pi^0}$ be the corresponding number of Monte Carlo mesons registered by the calorimeter and reconstructed and accepted by the analysis procedure in the interval $0.070 \leq m_{\gamma\gamma} \leq 0.190$ GeV. The detection acceptance factor is the ratio $\varepsilon_0 = (n_2/N_2)/(n_1/N_1)$.

In computing ε_0 , $n_1(E_{\pi^0})$ included all primary produced π^0 mesons and also those π^0 mesons produced by the decay of other particles with lifetimes less than 3.10^{-10} s. Note that ε_0 includes not only the geometrical and trigger acceptance but also accounts for fluctuations in the shower development, for overlap of clusters, for inefficiencies of the cluster search, and for radiative effects. In the barrel calorimeter the factor ε_0 varies between 0.04 and 0.13 for π^0 energies between 0.5 and 6 GeV, in the endcap calorimeter it is $\sim$ 0.10 above 2 GeV. The π^0 cross section has been computed from the measured number of accepted hadronic events, N_3, and the number of $\gamma\gamma$ combinations $n_3(E_{\pi^0})dE_{\pi^0}$, observed above background in the π^0 mass interval. The inclusive π^0 cross section is given by

$$\frac{d\sigma}{dE_{\pi^0}} = \sigma_T \cdot \frac{1}{\varepsilon_0} \cdot \frac{n_3(E_{\pi^0})}{N_3}$$

where σ_T is the total hadronic annihilation cross section measured in this experiment as 0.296 ± 0.015 nb (20).

3. Results

Table 2 shows the differential cross section $d\sigma/dp$ for inclusive π^0 production. Results from the barrel and the endcap calorimeters are shown separately. They agree within the errors. Above 6 GeV the data from the single cluster analysis in the barrel calorimeter were used, as described above. We show in addition the results from this method in the momentum interval 4.6-6.0 GeV. It agrees with the method used at lower energies at the point of overlap.

Table 2 shows statistical and systematic errors. In evaluating the systematic errors, the following contributions have been considered : uncertainties in background subtraction and energy calibration (typically 15 %, but 30 % above 10 GeV), acceptance (8 % for the barrel and 25 % for the endcap calorimeter), efficiency of the calorimeter (5 %) and luminosity measurement (5 %). All contributions were added in quadrature.

It should be noted, that the low energy point has a larger systematic uncertainty due to the difficulty of background subtraction. Table 3 and Figure 5 show the differential cross section with the data of the calorimeters combined. The errors have been computed by adding statistical and systematic errors in quadrature.

The new results agree well with those published previously on the basis of much lower statistics (4). In addition to the smaller errors obtained we have now considerably extended the momentum range of our π^0-measurement up to the highest kinematically allowed momenta. The new results are compared in Fig. 5 with the averages of the π^+ and π^- cross sections $(\sigma(\pi^+) + \sigma(\pi^-))/2$ as determined in (1). It can be seen that both momentum distributions agree over the whole measured range. The χ^2 value for this comparison is 13.2 for 7 d.o.f. (probability 7 %).

For the energy interval $0.7 \leq E_{\pi^0} \leq 17$ Gev for which π^0 and $\pi^\pm$ data are available

$$\frac{2 \cdot \sigma(\pi^0)}{\sigma(\pi^+) + \sigma(\pi^-)} = 1.13 \pm 0.18$$

The error covers statistical effects (± 0.12) , overall systematic effects (± 0.11) and errors from the $\pi^\pm$ cross section (± 0.072) , all added in quadrature.

In order to determine the total yield of π^0 mesons, the cross section has been extrapolated over the unobserved energy range.

$E_{\pi^0} \leq 0.7$ GeV by assuming that π^0 and $\pi^\pm$ have the same momentum distribution (20). This yields 5.8 ± 0.9 π^0 mesons per event, which is in agreement with other measurements (21,22) and can be compared to the charged pion rate of 10.3 ± 0.4 per event measured in this experiment (1).

The use of both calorimeters permits the measurement of the angular distribution over a large range. The corrected angular distribution integrated over the energy range $2.0 \leq E_{\pi^0} \leq 5.0$ GeV is shown in figure 6. The angular dependence can be parameterized as

$$\frac{d\sigma}{d\Omega} \sim 1 + A \cos^2\theta,$$

where $A = (\sigma_t - \sigma_\ell)/(\sigma_t + \sigma_\ell)$ can be related in the quark-parton model to the cross section contributions from transversely (σ_t) and longitudinally (σ_ℓ) polarized photons as seen in the π^0 rest system. A fit to the data where the statistical and systematic errors have been added in quadrature yields $A = 1.2 \pm 0.5$. Thus π^0 production above 2 GeV follows the angular distribution of the primary $q\bar{q}$ pairs (which is proportional to $1 + \cos^2\theta$). This observation is in agreement with our previous observations for charged hadrons (5).

Figure 7 compares the scaled cross section with results from other experiments 21,22,23,24). The agreement between the various measurements is good. It should be noted that for all experiments the systematic error at low values of $\langle x \rangle$ are large compared to the statistical errors.

In summary, we have measured the inclusive cross section for π^0 meson production at 34.6 GeV center of mass energy. Due to the fine granularity of the liquid argon calorimeter the spectrum could be extended to the largest kinematically allowed π^0 momenta. The shapes of the momentum distributions for π^0 and for $\pi^\pm$ mesons agree in the momentum interval 0.7-17 GeV. In that interval we measure the ratio $2\sigma(\pi^0)/(\sigma(\pi^+) + \sigma(\pi^-)) = 1.13 \pm 0.18$. Assuming that π^0 and $\pi^\pm$ mesons have the same momentum distribution below 0.7 GeV, and using the multiplicity of $\pi^\pm$ -mesons as measured in this experiment, we find a mean π^0 multiplicity of 5.8 ± 0.9. The angular distribution of π^0 mesons was measured over a large range using the barrel and endcap calorimeters. We find $d\sigma/d\Omega \sim 1 + A \cos^2\Theta$ with $A = 1.2 \pm 0.5$.

Acknowledgments

We gratefully acknowledge the effort of the PETRA machine group and the support of the DESY directorate. We are pleased to thank Professor Paul Söding for his earlier contributions to this experiment. Those of us from abroad wish to thank the DESY directorate for the hospitality extended to us.

Figure captions

Figure 1 The $\gamma\gamma$ mass distributions with photon energies $E_\gamma > 0.150$ GeV for
a) $0.5 \leq E_{\gamma\gamma} < 4$ GeV in the barrel calorimeter,
b) $2 < E_{\gamma\gamma} < 6$ GeV in the barrel calorimeter, and
c) $1.5 < E_{\gamma\gamma} < 5$ GeV in the endcap calorimeter. The dashed curves show the estimate of background contribution calculated by Monte Carlo methods. The solid curves show the Monte-Carlo calculation of signal plus background.

Figure 2 Projected shower width D_ϕ vs D_z for
a) single photons (data)
b) single clusters from π^0 (Monte Carlo)
c) single clusters from hadronic events (data)

Figure 3 Normalized distribution of R^2 (R = normalized shower width, see text)
a) single photons (data from $e^+e^- \to \gamma\gamma$)
b) single clusters from (Monte Carlo)
c) single clusters from hadronic events (data)

Figure 4 The background subtracted $\gamma\gamma$ mass distribution for
a) $0.5 < E_{\gamma\gamma} < 4$ GeV in the barrel calorimeter,
b) $2 < E_{\gamma\gamma} < 6$ GeV in the barrel calorimeter, and
c) $1.5 < E_{\gamma\gamma} < 5$ GeV in the endcap calorimeter. The solid curves show the fit results of a gaussian distribution to the signal.

Figure 5 The differential cross section $d\sigma/dp$ for $e^+e^- \to \pi^0$ + anything. The errors have been computed by adding statistical and systematic errors in quadrature. For comparison also the cross section $(d\sigma(\pi^+)/dp + d\sigma(\pi^-)dp)/2$ is shown.

Figure 6 The corrected angular distribution for π^0 production integrated over the energy range $2.0 < E_{\pi^0} < 5.0$ GeV. Overall normalisation error not included.

Figure 7 The scaled cross section $(s/\beta)d\sigma/dx$ for $e^+e^- \to \pi^0$ + anything at 34.6 GeV c.m. energy. The results from the barrel and endcap calorimeters have been combined. For comparison, results from CELLO at 34 GeV, from the PEP-4 TPC at 29 GeV and from JADE at 34 GeV are shown. For CELLO, points from "Method A" are shown for $x < 0.4$, and from "Method B" for $x > 0.4$. For PEP-4 TPC, R has been assumed to be 4.00 at 29 GeV for the purposes of comparison. The errors shown are statistical and systematic added in quadrature.

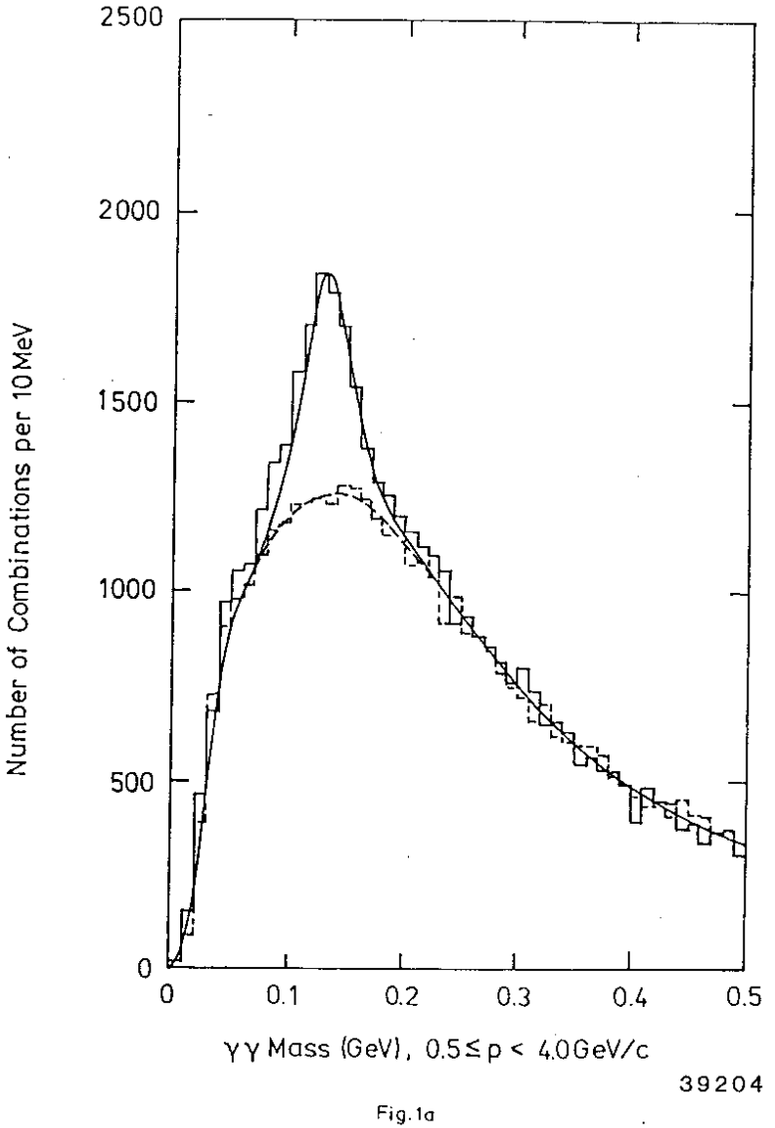

Fig.1a

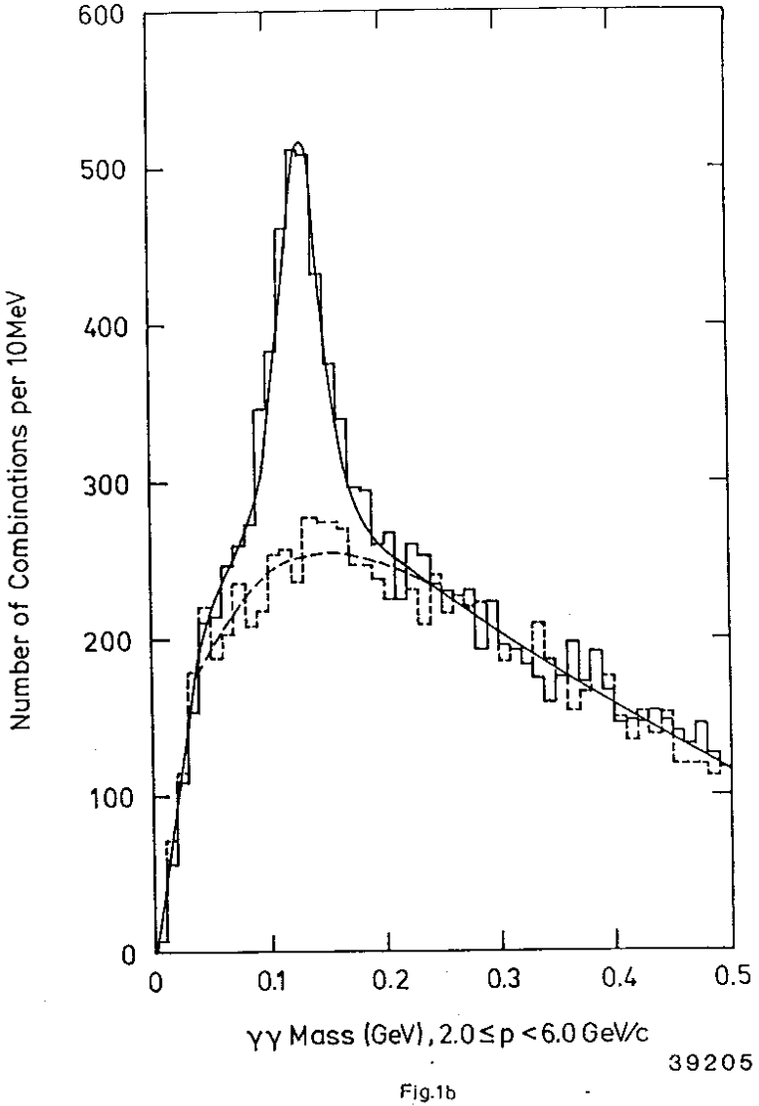
600
500
400
300
200
100
0
0
0.1
0.2
0.3
0.4
0.5
Number of Combinations per 10MeV
γγ Mass (GeV), 2.0≤p<6.0 GeV/c
39205

Fig.1b

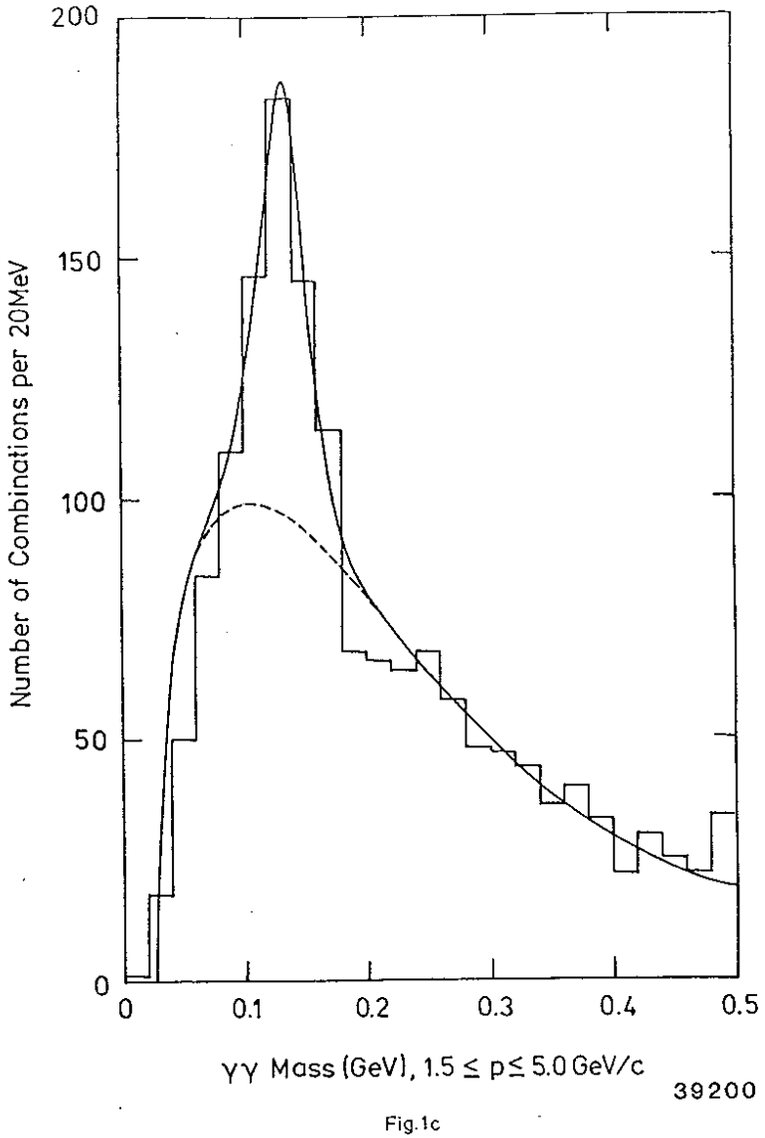
200
150
100
50
0
0
0.1
0.2
0.3
0.4
0.5
Number of Combinations per 20MeV
γγ Mass (GeV), 1.5 ≤ p≤ 5.0 GeV/c
39200

Fig.1c

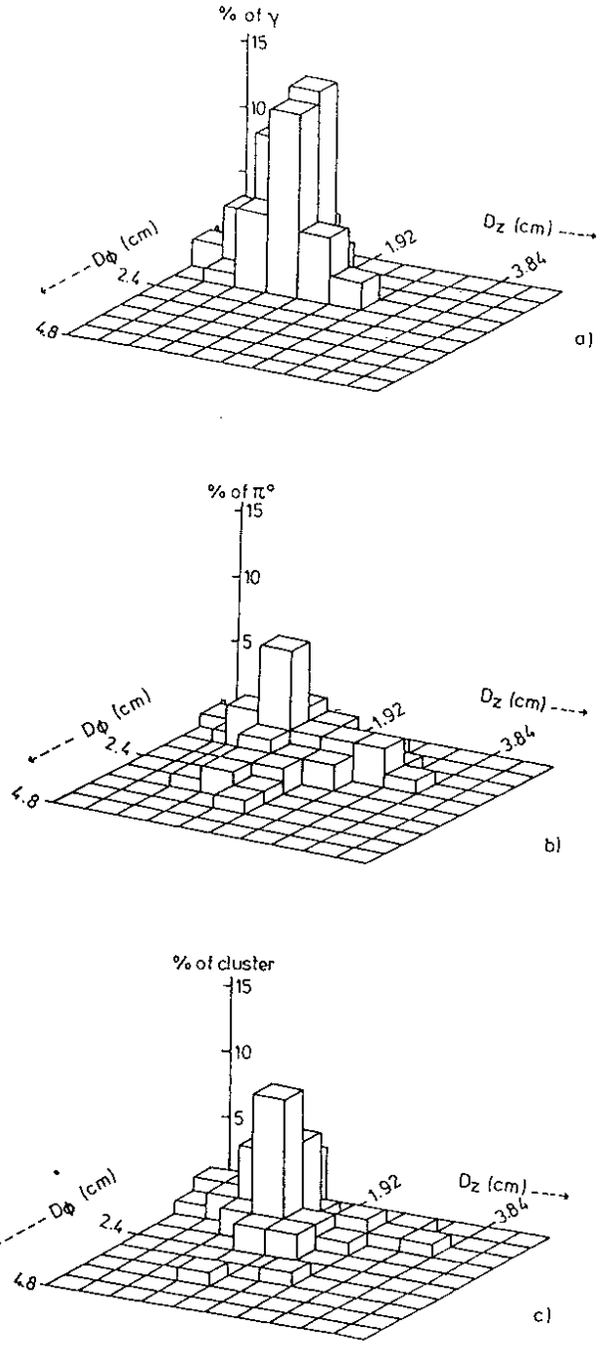
% of γ
15
10
Dφ (cm)
2.4
4.8
1.92
Dz (cm)
3.84
a)
% of π°
15
10
5
Dφ (cm)
2.4
4.8
1.92
Dz (cm)
3.84
b)
% of cluster
15
10
5
Dφ (cm)
2.4
4.8
1.92
Dz (cm)
3.84
c)

Fig. 2

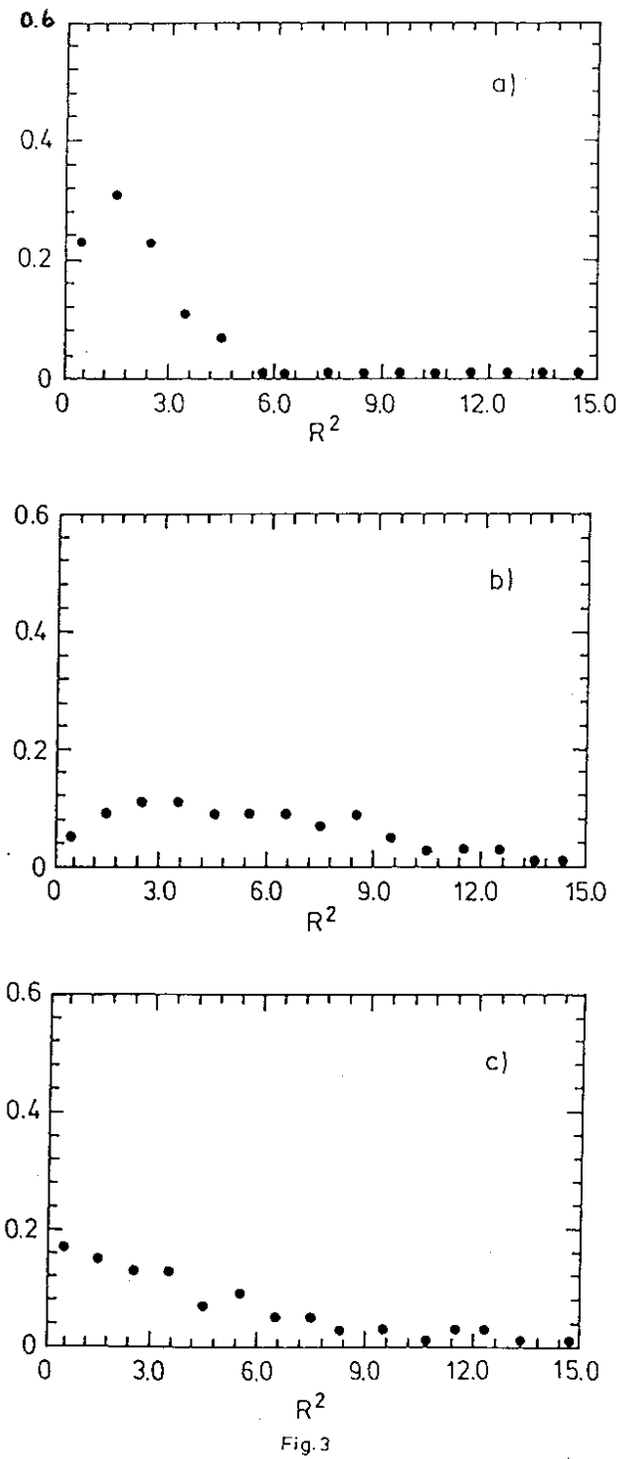
0.6
0.4
0.2
0
a)
0
3.0
6.0
9.0
12.0
15.0
R²
0.6
0.4
0.2
0
b)
0
3.0
6.0
9.0
12.0
15.0
R²
0.6
0.4
0.2
0
c)
0
3.0
6.0
9.0
12.0
15.0
R²

Fig. 3

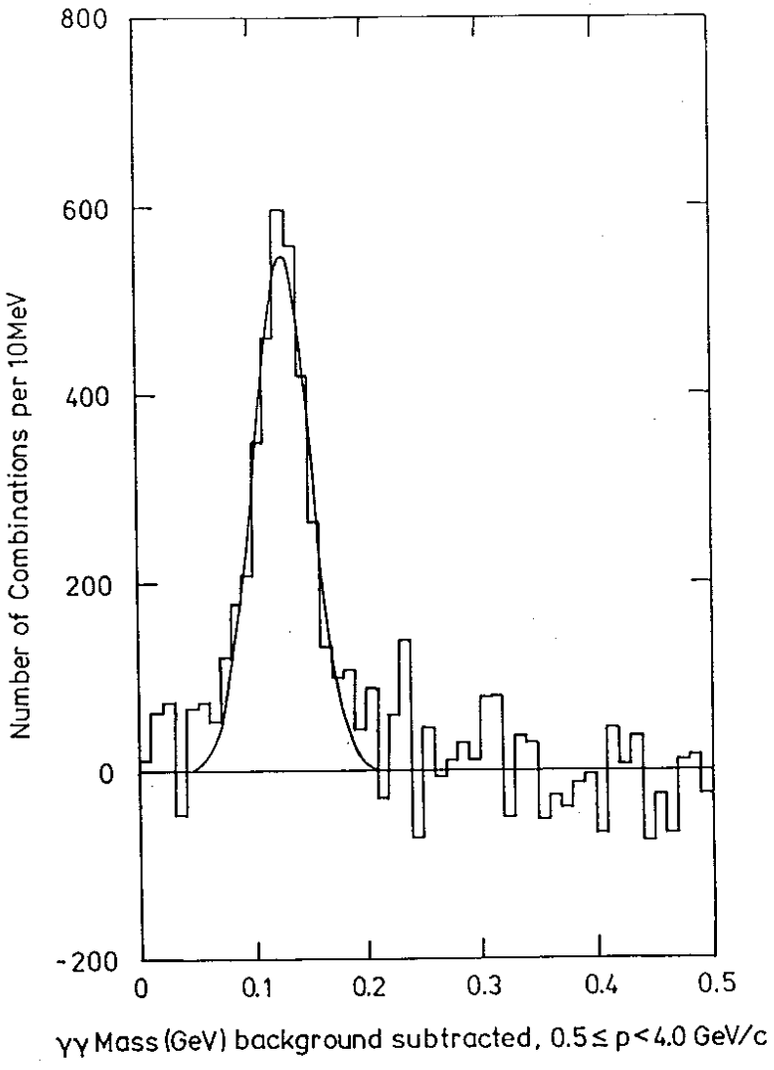
800
600
400
200
0
-200
0
0.1
0.2
0.3
0.4
0.5
Number of Combinations per 10MeV
γγ Mass (GeV) background subtracted, 0.5 ≤ p < 4.0 GeV/c
39206

Fig.4a

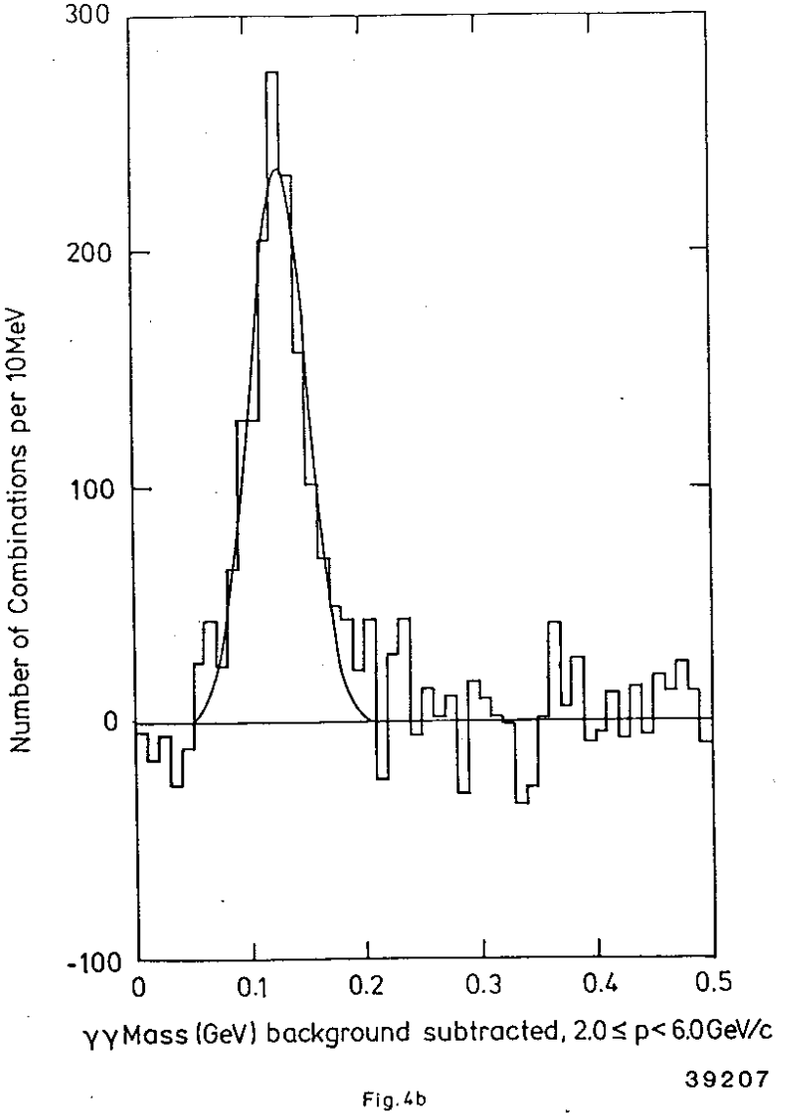
300
200
100
0
-100
0
0.1
0.2
0.3
0.4
0.5
Number of Combinations per 10MeV
γγ Mass (GeV) background subtracted, 2.0 ≤ p < 6.0 GeV/c
39207

Fig.4b

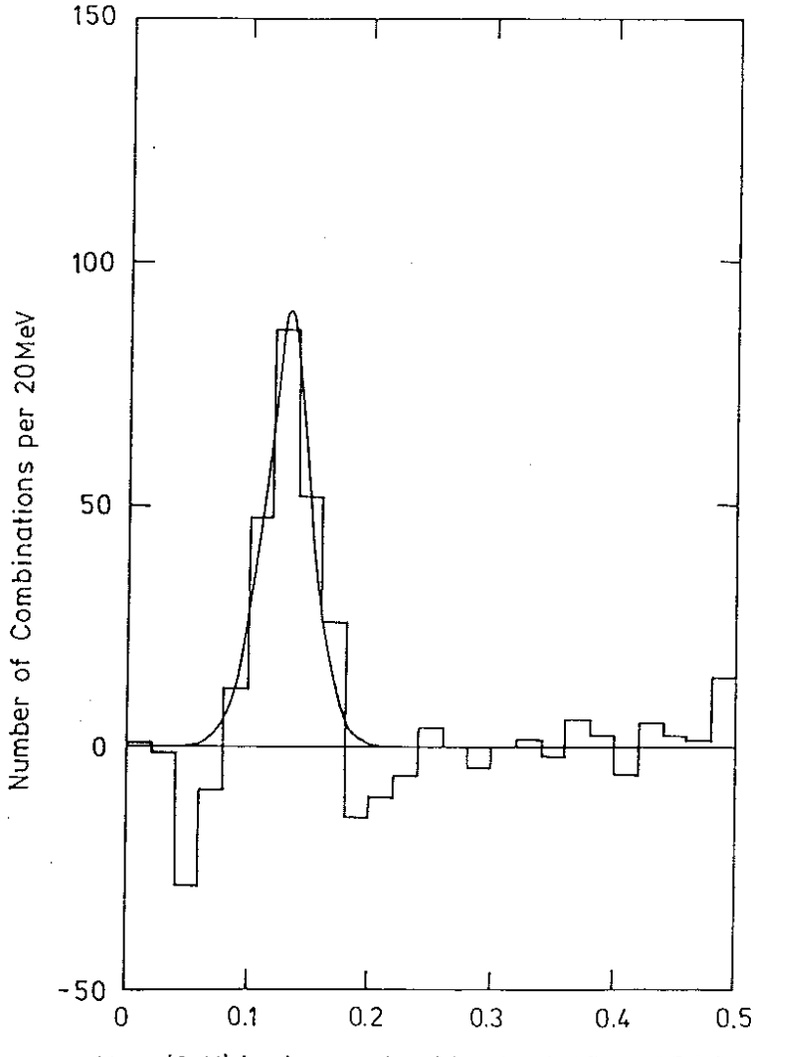
150
100
50
0
-50
0
0.1
0.2
0.3
0.4
0.5
Number of Combinations per 20MeV
γγ Mass (GeV) background subtractred, 1.5 ≤ p ≤ 5.0 GeV/c
39201

Fig.4c

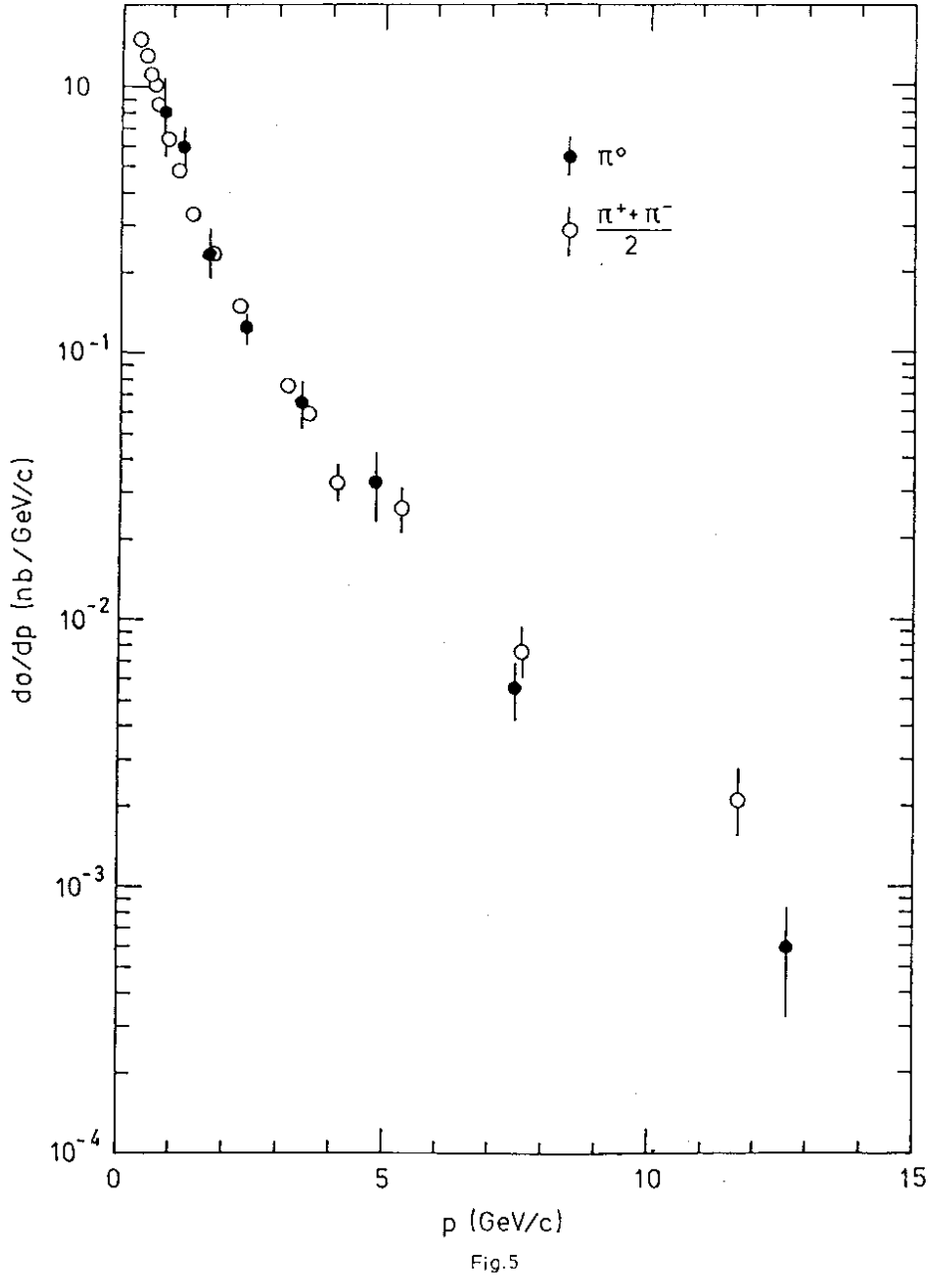
10
10^{-1}
10^{-2}
10^{-3}
10^{-4}
0
5
10
15
dσ/dp (nb/GeV/c)
p (GeV/c)
π°
$\frac{\pi^+ + \pi^-}{2}$

Fig.5

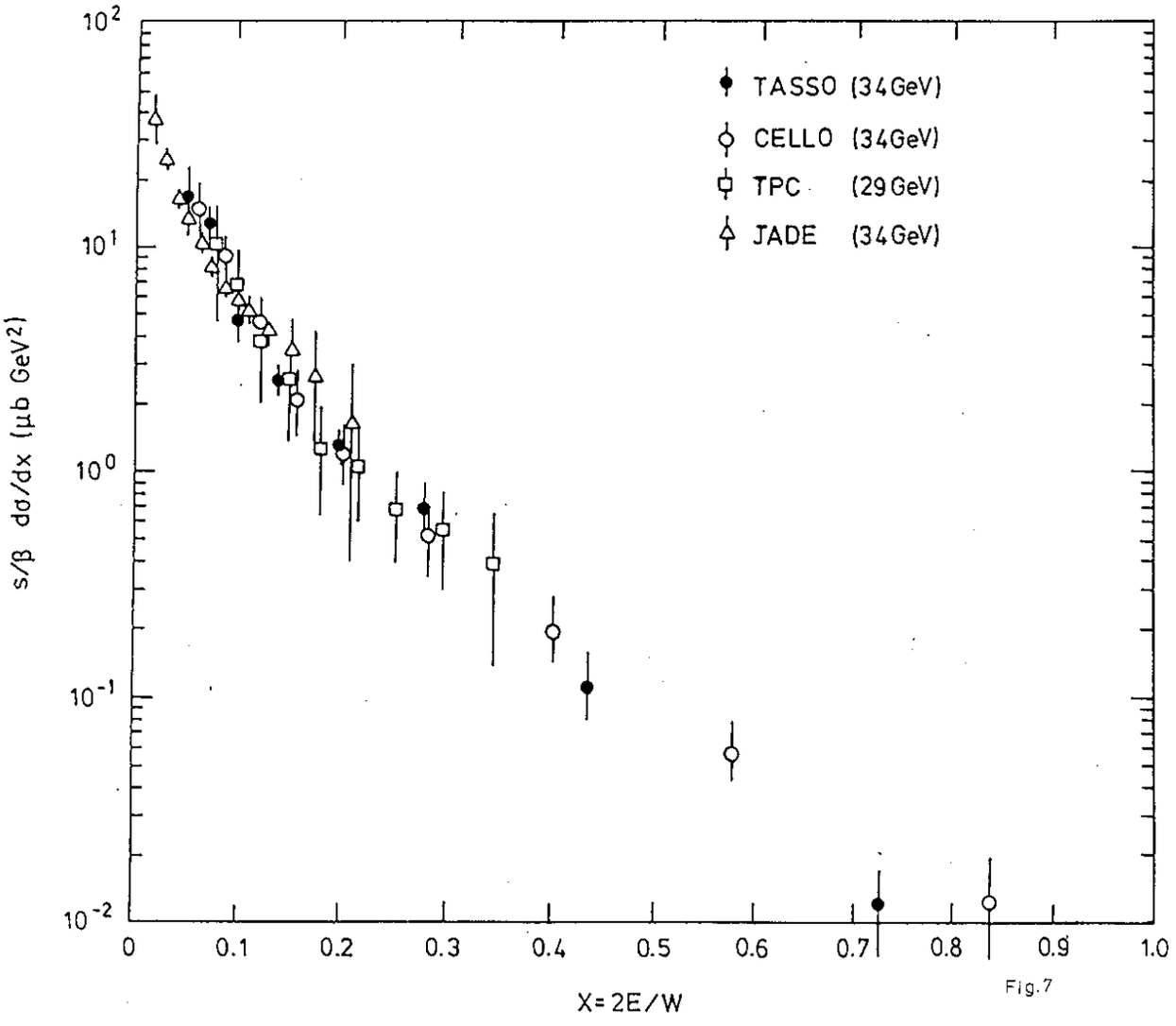
TASSO (34GeV)
CELLO (34GeV)
TPC (29GeV)
JADE (34GeV)
s/β dσ/dx (μb GeV²)
X= 2E/W

Fig.7

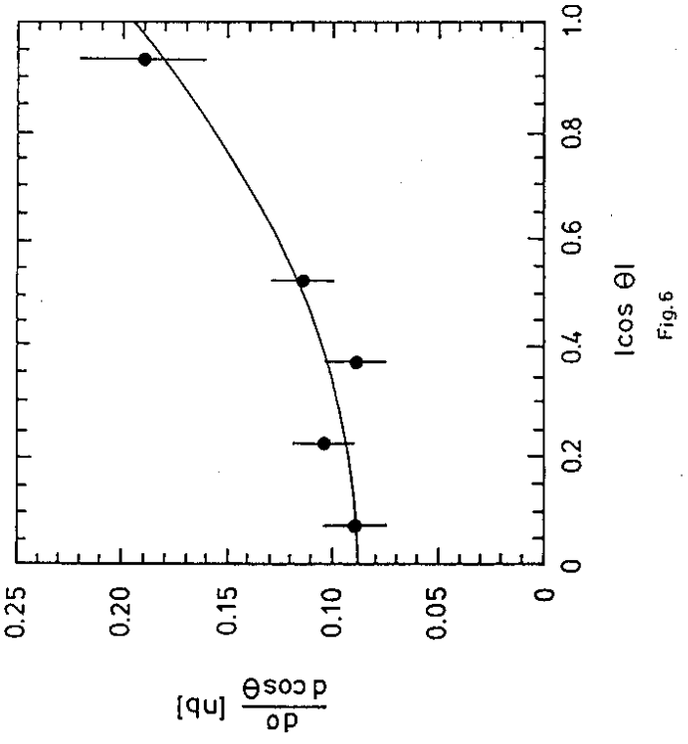
dσ/d cosθ [nb]
|cos θ|

Fig.6

Table 1

Results for the cross section $d\sigma/dE$ (nb/GeV) obtained by cluster width methods (sect. 2.2.2.)

Energy Range

Method	$d\sigma/dE$ for 4<E< 4.6 GeV	$d\sigma/dE$ for 4.6<E<6 GeV	$d\sigma/dE$ for 6<E<10 GeV	$d\sigma/dE$ for 10<E<17 GeV
Two-dimensional fit D_ϕ vs D_z	0.07 ± 0.06	0.021 ± 0.009	0.0055±0.0006	0.00057 ± 0.00014
Fit to R^2 distribution	-	0.027	0.0050	0.00024
Two-dimensional fit, 4th moment of $D_{\phi,z}$ distributions	0.04 ± 0.04	0.019 ± 0.010	0.0048±0.0013	0.00032 ± 0.00015
cuts in in D_ϕ and D_z D_ϕ = 2.37 cm D_z = 2.49 cm	0.032	0.022	0.0058	0.0007
D_ϕ = 2.13 cm D_z = 2.36 cm	0.031	0.022	0.0056	0.0006

Table 2 : The differential cross section $d\sigma/dp$ for $e^+e^- \to \pi^0$ + anything at 34.6 GeV center of mass energy. Statistical and systematic errors are given.

Barrel Calorimeter

momentum range (GeV/c)	$d\sigma/dp$ (nb/GeV/c)			remarks
0.7-1.0	0.82	± 0.12	± 0.25	
1.0-1.5	0.59	± 0.05	± 0.11	
1.5-2.0	0.251	± 0.027	± 0.043	use π^0 mass
2.0-3.0	0.122	± 0.011	± 0.015	distribution
3.0-4.0	0.060	± 0.007	± 0.010	
4.0-6.0	0.033	± 0.004	± 0.008	
4.6-6.0	0.021	± 0.009	± 0.004	use single
6.0-10.0	0.0056	± 0.0006	± 0.0012	clusters
10.0-17.0	0.00058	± 0.00014	± 0.00020	

Endcap Calorimeter

momentum range (Gev/c)	$d\sigma/dp$ (nb/GeV/c)
1.5-2.0	0.156 ± 0.082 ± 0.078
2.0-3.0	0.135 ± 0.038 ± 0.038
3.0-4.0	0.086 ± 0.025 ± 0.025
4.0-5.0	0.056 ± 0.018 ± 0.017

Table 3 : The differential cross section $d\sigma/dp$ for $e^+e^- \to \pi^0$ + anything at 34.6 GeV center of mass energy. Data from all calorimeters combined, statistical and systematic errors have been added in quadrature.

momentum range (GeV/c)	<p> (GeV/c)	$d\sigma/dp$ (nb/GeV/c)
0.7-1.0	0.83	0.82 ± 0.28
1.0-1.5	1.22	0.59 ± 0.12
1.5-2.0	1.73	0.24 ± 0.05
2.0-3.0	2.43	0.124 ± 0.018
3.0-4.0	3.45	0.063 ± 0.011
4.0-6.0	4.85	0.033 ± 0.009
6.0-10.0	7.5	0.0056 ± 0.0013
10.0-17.0	12.6	0.0006 ± 0.0003

Table 4 : The scaled cross section $(s/\beta)d\sigma/dx$ for $e^+e^- \to \pi^0$ + anything at 34.6 GeV center of mass energy. Statistical and systematic errors are added in quadrature, $x = 2 E_{\pi^0}/\sqrt{s}$, $\sqrt{s}$ = CM energy.

energy range (GeV)	<x>	$(s/\beta)d\sigma/dx$ (μb GeV^2)
0.7-1.0	0.048	17.6 ± 6.0
1.0-1.5	0.071	12.7 ± 2.4
1.5-2.0	0.100	4.9 ± 1.0
2.0-3.0	0.140	2.54 ± 0.38
3.0-4.0	0.199	1.29 ± 0.23
4.0-6.0	0.280	0.68 ± 0.19
6.0-10.0	0.434	0.115 ± 0.027
10.0-17.0	0.728	0.012 ± 0.005

References

1) TASSO Collaboration, M. Althoff et al., Z. Phys. C17 (1983) 5
2) TASSO Collaboration, R. Brandelik et al., Phys. Lett. 113B (1982) 98
3) Tasso collaboration, M, Althoff et al., Z. Phys. C27 (1985) 27
4) Tasso Collaboration, R. Brandelik et al., Phys. Lett. 108B (1982) 261
5) TASSO Collaboration, R. Brandelik et al., Phys. Lett. 113B (1982) 499
6) TASSO Collaboration, R. Brandelik et al., Phys. Lett. 114B (1982) 65
7) TASSO Collaboration, R. Brandelik et al., Phys. Lett. 83B (1979) 261

8) TASSO Collaboration, M. Althoff et al., Phys. Lett. 146B (1984) 443
9) TASSO Collaboration, M. Althoff et al., Z. Phys. C26 (1984) 337
10) V. Kadansky et al., Physica Scripta 23 (1981) 680
11) R.L. Ford and W.R. Nelson, SLAC Report 210 (1978)
12) E. Wicklund, PhD. Thesis University of Wisconsin (1984)
13) G.Tysarczyk , Diplom thesis, Hamburg 1986

14) E. Vogel, Diplom Thesis, Aachen 1984, AC-Intern 84/08
15) H. Fesefeldt, Aachen PITHA report 85-02
16) P. Hoyer et al., Nucl. Phys. B161 (1979) 349
17) R.D. Field and R.P. Feynman, Nucl. Phys. B136 (1978) 1
18) A. Berends and R. Kleiss, Nucl. Phys. B178 (1981) 141
19) A. Grant, Nucl. Instr. Meth. 131 (1975) 167
20) TASSO Collaboration, M. Althoff et al., Z. Phys. C22 (1984) 307
21) PEP-4 TPC Collaboration, H. Aihara et al., Z. Phys. C27 (1985) 187
22) JADE Collaboration, W. Bartel et al., Z. Phys. C28 (1985) 343
23) CELLO Collaboration, H.J. Behrend et al., Z. Phys. C14 (1982) 189
24) CELLO Collaboration, H.J. Behrend et al., Z. Phys. C20 (1983) 207